analysis of the kinetic data difficult, if not impossible.

The absence of a kinetic isotope effect suggests (but does not prove) that proton transfer occurs after the rate-determining formation of a 5-coordinate intermediate (eq 18). This mech-

$$\begin{array}{l} OAs(OR)_3 + R'OH \rightleftarrows OAs(OR)_3(OHR') \\ \qquad\qquad\qquad\qquad \updownarrow \\ OAs(OR)_2(OR') + ROH \rightleftarrows OAs(OR)_2(OR')(OHR) \end{array} \quad (18)$$

anism requires that proton transfer between alkoxyl groups of the trigonal-bipyramidal intermediate, probably accompanied by pseudorotation,[21] be fast compared with dissociation of the intermediate. Such a postulate is consistent with the activation parameters which suggest essentially no bond breaking in the transition state. The intermediate is not a significant equilibrium species, however; NMR spectra showed no extra resonances and careful measurements showed that the α- and β-proton chemical shifts of isopropyl alcohol and triisopropyl arsenate were independent, respectively, or ester and alcohol concentrations.

The mechanism of the acid-catalyzed exchange process presents an interesting problem. A catalyst which operates by lowering the entropic contribution to the free energy of activation while increasing the enthalpic contribution is at least unusual. The exchange kinetics are cleanly first order in *p*-toluenesulfonic acid in the concentration range studied, 0.02–0.37 M. Measurement of the conductance of solutions of the acid in acetonitrile showed that the molar conductivity is small and very nonlinear in this concentration range.[3] Thus we conclude that the observed catalysis involves the undissociated acid.

Chemical shift experiments described above suggest that the catalyst is largely hydrogen bonded to the ester in the concentration range used in the kinetic experiments. It seems reasonable to suppose, therefore, that alcohol exchange with the ester–catalyst hydrogen-bonded complexes E·C, E·2C, and E·A·C proceeds faster than when the ester is free of hydrogen bonds or is associated only with alcohol molecules. The acid is expected to be a better hydrogen-bond donor, and this is reflected in the larger formation constant obtained from the chemical shift data. Hydrogen bonding to the unique ester oxygen might be expected to weaken the As=O bond, thereby facilitating the formation of a 5-coordinate intermediate. However, this cannot be the major catalytic effect since one would then expect the reaction to be catalyzed by alcohol as well. This inductive effect in either case would be partially compensated by increased steric crowding in formation of a 5-coordinate transition state or intermediate. The difference in behavior of the ester–acid and ester–alcohol hydrogen-bonded complexes must be due to the ability of the sulfonic acid to facilitate proton transfer.

The kinetic isotope effect found for the acid-catalyzed-exchange process suggests that proton transfer occurs in this case prior to the transition state. If formation of the 5-coordinate transition state is accompanied by at least partial transfer of the alcohol proton to one of the sulfonate oxygens, the system is set up for pseudo-rotation accompanied by shift of the proton to another alkoxyl group. Indeed, there seems to be nothing to prevent the entire process from being concerted. Such a mechanism is consistent with the activation parameters which suggest a looser transition state with relatively less As-O bond formation (and more As-O bond breaking) than in the uncatalyzed pathway. The effect of the catalyst apparently is to merge the proton-transfer step into the formation of the 5-coordinate species, thus destabilizing the intermediate and speeding the exchange process.

Acknowledgments. This work was supported by Grant number ES-00894 from the National Institute of Environmental Health Sciences.

Supplementary Material Available: Observed lifetimes for arsenate triester–alcohol exchange from NMR data for methyl, ethyl, *n*-propyl, *n*-butyl, and *n*-pentyl alcohols (5 pages). Ordering information is given on any current masthead page.

(21) Westheimer, F. H. *Acc. Chem. Res.* **1968**, *1*, 70–77.

A Semiclassical Treatment of Electron-Exchange Reactions. Application to the Hexaaquoiron(II)–Hexaaquoiron(III) System

Bruce S. Brunschwig, Jean Logan, Marshall D. Newton,* and Norman Sutin*

Contribution from the Chemistry Department, Brookhaven National Laboratory, Upton, New York 11973. *Received March 17, 1980*

Abstract: A semiclassical description of electron-exchange reactions, in which a classical treatment of the solvent motion is combined with a quantum-mechanical description of the inner-sphere modes, is developed. This approach, which assumes that the solvent and inner-sphere reorganizations can be treated independently, yields relatively simple expressions for the variation of the electron-exchange rate constant and activation parameters with temperature. The semiclassical description is compared with the classical Marcus–Hush theory and with the quantum-mechanical theory of Kestner, Logan, and Jortner. The semiclassical formalism is remarkably successful in reproducing the results of the full quantum-mechanical theory at all temperatures. Both theories yield activation parameters that approach the classical values at high temperature. The activation parameters for the $Fe(H_2O)_6^{2+}$–$Fe(H_2O)_6^{3+}$ exchange reaction predicted by the various theories are compared with the experimental results. The calculations show that at 300 K the free energy of activation is close to the value predicted by the classical model despite the fact that the average energy of the reacting species is significantly less than the classical barrier.

Introduction

Electron transfer is of importance in a variety of physical, chemical, and biological systems, ranging from semiconductors to cytochromes.[1,2] Rates of electron transfer in these systems span some 20 orders of magnitude. There is a continuing interest in the origins of this large rate variation and both classical[3,4] and

(1) Chance, B., DeVault, D. C., Frauenfelder, H., Marcus, R. A., Schrieffer, J. B., Sutin, N., Eds. "Tunneling in Biological Systems"; Academic Press: New York, 1979.

(2) Reynolds, W. L.; Lumry, R. W. "Mechanisms of Electron Transfer"; Ronald Press: New York, 1966. Addison, A. W.; Cullen, W. R.; Dolphin, D.; James, B. R. "Biological Aspects of Inorganic Chemistry"; Wiley-Interscience: New York, 1977.

(3) Marcus, R. A. *Discuss. Faraday Soc.* **1960**, *29*, 21. *Annu. Rev. Phys. Chem.* **1964**, *15*, 155. *J. Chem. Phys.* **1965**, *43*, 679. *Electrochim. Acta* **1968**, *13*, 995.

0002-7863/80/1502-5798$01.00/0

quantum-mechanical[5-10] interpretations have been proposed. In this article we show how various components of these treatments can be combined within a semiclassical framework and we apply the different approaches to outer-sphere electron-exchange reactions of metal complexes. Outer-sphere electron-exchange reactions

$$ML_6^{3+} + ML_6^{2+} \overset{k_{ex}}{\rightleftharpoons} ML_6^{2+} + ML_6^{3+} \quad (1)$$

constitute the simplest class of electron-transfer reactions because no bonds are made or broken during the course of the reaction and because the reactants and products of exchange reactions are identical. Moreover, because of the symmetry of the reactions the driving force (energy gap) for the electron transfer is zero and the properties of only one redox couple ($ML_6^{3+/2+}$) rather than those of two different redox couples need to be considered. As a consequence the theoretical expressions are greatly simplified and differences between the various treatments are more readily evident.

Studies of bimolecular electron-transfer processes have shown that reactions such as eq 1 occur in a number of steps:[11,12]

$$ML_6^{3+} + ML_6^{2+} \overset{K_0}{\rightleftharpoons} ML_6^{3+}|ML_6^{2+} \quad (2)$$

$$ML_6^{3+}|ML_6^{2+} \overset{k_{el}}{\rightleftharpoons} ML_6^{2+}|ML_6^{3+} \quad (3)$$

$$ML_6^{2+}|ML_6^{3+} \overset{K_0^{-1}}{\rightleftharpoons} ML_6^{2+} + ML_6^{3+} \quad (4)$$

The first step is the formation of a precursor complex from the separated reactants (eq 2). The actual electron transfer occurs within the precursor complex to form a successor complex (eq 3). The dissociation of the successor complex into separated products occurs in the third step (eq 4). Provided that the formation of the precursor complex is not rate determining, k_{ex}, the observed rate constant for the electron exchange, is equal to K_0k_{el}[13] where K_0 is the equilibrium constant for the formation of the precursor complex (eq 2) and k_{el} is the first-order rate constant for electron transfer within the precursor complex (eq 3). Various expressions for K_0 have been proposed. These have been discussed elsewhere[11,13] and will not be considered here. Instead we focus on the rate of electron transfer within the precursor complex.

Electron transfer within a (weak-interaction) precursor complex is governed by the Franck–Condon principle.[1,14] According to this principle, internuclear distances and nuclear velocities do not change during an electronic transition; in other words, the actual electron transfer occurs at essentially constant nuclear configuration and momentum. The Franck–Condon principle is embodied in a different manner in the classical and quantum-mechanical electron-transfer theories. In the classical theories[3,4,15] an activated-complex formalism is generally used. Since the activated complex for the electron transfer occurs at the intersection of two potential-energy surfaces—one for the reactants and the other for the products—the Franck–Condon principle is obeyed (the nuclear configurations and energies of the reactants and products are the same at the crossing point). On the other hand, in the quantum-mechanical theories[5-10,16] the intersection of the potential-energy surfaces is deemphasized and the electron transfer is treated as a radiationless transition between the reactant and product states. Time-dependent perturbation theory is used, and the restrictions on the nuclear configurations for electron transfer are measured by the square of the overlap of the vibrational wave functions of the reactants and products (i.e., by the Franck–Condon factors for the transition).

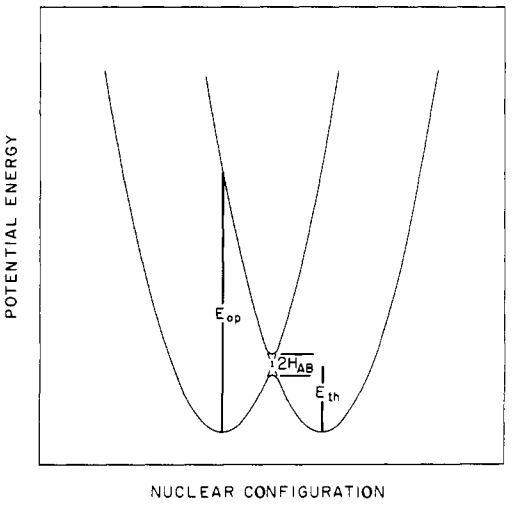

Figure 1. Plot of the potential energy of the reactants and products of an electron-exchange reaction as a function of nuclear configuration: E_{op} is the energy for the light-induced electron transfer and E_{th} is the activation energy for the thermal electron transfer. For parabolic curves the abscissa corresponds to the straight line in N dimensions connecting the reactants' and products' potential-energy minima.

In this paper we dissect the electron-transfer rate expressions arising from the classical and quantum-mechanical theories, and develop a semiclassical model. The latter combines the simplicity of the classical approach with some of the essential features of the full quantum-mechanical theory. In particular, the rate constant for electron transfer in the semiclassical model can be related to the classical rate constant by introducing a thermally averaged electronic transmission coefficient κ_{el} and a thermally averaged nuclear tunneling factor Γ_n:

$$k_{sc} = \kappa_{el}\Gamma_n k_{cl} \sim k_{qm} \quad (5)$$

The departure of the electronic transmission coefficient from unity is generally interpreted as nonadiabatic behavior. Four cases can be distinguished depending on the values of κ_{el} and Γ_n: (a) simple adiabatic ($\kappa_{el} = 1$, $\Gamma_n = 1$), (b) simple nonadiabatic ($\kappa_{el} \neq 1$, $\Gamma_n = 1$), (c) adiabatic with nuclear tunneling ($\kappa_{el} = 1$, $\Gamma_n \neq 1$), and (d) nonadiabatic with nuclear tunneling ($\kappa_{el} \neq 1$, $\Gamma_n \neq 1$).

The remainder of this paper is divided into four parts. In the first part the classical activated-complex rate expressions are presented; these correspond to case (a) above. Case (b) is considered in the second part. The rate constants derived for case (d) by using first-order time-dependent perturbation theory are presented next. In the fourth part we develop the semiclassical description and generalize it to include case (c). The validity and utility of the various approaches are assessed in detail for the $Fe(H_2O)_6^{2+}$–$Fe(H_2O)_6^{3+}$ electron-exchange reaction, for which extensive numerical results are presented.

I. Classical Models

The potential energy of the reactants may be represented by an N-dimensional surface in $(N + 1)$-dimensional space where N is the number of independent variables necessary to define the configuration of the coordination shells of the reactants.[3,15] This surface will have valleys corresponding to the more stable nuclear configurations of the reactants. The potential energy of the products may be represented by a similar surface in the $(N +$

(4) Hush, N. S. *Trans Faraday Soc.* **1961**, *57*, 155.
(5) Holstein, T. *Philos. Mag.* **1978**, *37*, 49. *Ann. Phys. (Leipzig)* **1959**, *8*, 343. In ref 1, p 129.
(6) Levich, V. G. *Adv. Electrochem. Electrochem. Eng.* **1966**, *4*, 249.
(7) Kestner, N. R.; Logan, J.; Jortner, J. *J. Phys. Chem.* **1974**, *78*, 2148.
(8) Ulstrup, J.; Jortner, J. *J. Chem. Phys.* **1975**, *63*, 4358. Efrima, S.; Bixon, M. *Chem. Phys.* **1976**, *13*, 447. Van Duyne, R. P.; Fischer, S. F. *Chem. Phys.* **1974**, *5*, 183.
(9) Hopfield, J. J. *Proc. Natl. Acad. Sci. U.S.A.* **1974**, *71*, 3640.
(10) Vorotyntsev, M. A.; Dogonadze, R. R.; Kuznetsov, A. M. *Dokl. Akad. Nauk SSSR* **1970**, *195*, 1135. German, E. D.; Dvali, V. G.; Dogonadze, R. R.; Kuznetsov, A. M. *Elektrokimiya* **1976**, *12*, 639. Dogonadze, R. R.; Kuznetsov, A. M. *Prog. Surf. Sci.* **1975**, *6*, 1. *Elektrokimiya* **1967**, *2*, 1324. Dogonadze, R. R.; Kuznetsov, A. M.; Levich, V. G. *Electrochim. Acta* **1968**, *13*, 1025.
(11) Brown, G. M.; Sutin, N. *J. Am. Chem. Soc.* **1979**, *101*, 883.
(12) Sutin, N. *Acc. Chem. Res.* **1968**, *1*, 225.
(13) Sutin, N. In ref 1, p 201.
(14) Libby, W. F. *J. Phys. Chem.* **1952**, *56*, 863.
(15) Sutin, N. *Annu. Rev. Nucl. Sci.* **1962**, *12*, 285.
(16) Ulstrup, J. "Charge Transfer Processes in Condensed Media"; Springer-Verlag: West Berlin, 1979.

1)-space. This surface will have its own valleys, corresponding to the more stable nuclear configurations of the products. The valleys in the reactants' potential-energy surface will generally occur at different nuclear coordinates from those in the products' potential-energy surface. This is due to the differing charge and size of the two reactants.

In the absence of interaction between the orbitals of the reactants the two potential-energy surfaces will intersect on an $(N-1)$-dimensional surface on which the reactants and products have the same configurations and the same total energies. A cross section of two intersecting potential-energy surfaces (assumed to be harmonic) is shown in Figure 1. If there is interaction between the reactants, the degeneracy at the intersection will be removed and two new surfaces will be formed. The separation between the two surfaces is equal to $2H_{AB}$ where H_{AB} is the interaction energy (electronic coupling matrix element).[3,15]

As discussed in the Introduction, the electron transfer in the activated-complex formalism occurs in the intersection region.[3,17] In the classical theories the interaction energy is assumed to be large enough so that the reactants are converted into products with unit probability in the intersection region, but small enough so that it can be neglected in calculating the amount of energy required to reach the intersection region. The latter is reached by a suitable fluctuation in the nuclear configurations of the reactants. If E_{th} is the potential energy required to change the nuclear coordinates of the reactants from their equilibrium values to the coordinates appropriate to the intersection region (i.e., E_{th} is the barrier for the thermal electron-transfer reaction), then the rate constant for electron exchange in the high-temperature limit is given by[3]

$$k_{el} = \nu_n e^{-E_{th}/RT} \tag{6}$$

where ν_n, the effective vibration frequency of the reactants, is defined by the parabolic curves in Figure 1. For many purposes it is convenient to relate the rate constants to a vertical or optical energy defined as the difference between the energies of the reactants and products at the equilibrium configuration of the reactants. If this difference is denoted by E_{op} (Figure 1) then $E_{op} = 4E_{th}$ if, as in Figure 1, the relevant potential-energy curves are parabolic.

The reorganization energy is made up of two parts, the inner-shell and the outer-shell (solvent) reorganization energy:

$$E_{th} = E^*_{in} + E^*_{out} \tag{7a}$$

$$E_{op} = E_{in} + E_{out} \tag{7b}$$

$$\Delta G^*_\lambda = \Delta G^*_{in} + \Delta G^*_{out} \tag{8}$$

In eq 8 ΔG^*_λ is the free energy required to reorganize the reactants prior to electron transfer.[18] The relationship between these quantities will be illustrated by considering the reorganization of the precursor complex in the $Fe(H_2O)_6^{2+}$–$Fe(H_2O)_6^{3+}$ exchange reaction:

$$Fe(H_2O)_6^{2+}|Fe(H_2O)_6^{3+} \rightleftarrows Fe(H_2O)_6^{3+}|Fe(H_2O)_6^{2+} \tag{9}$$

Provided that the metal–ligand vibrations are harmonic (at least to the intersection region), the inner-shell reorganization energy can be estimated from the equilibrium bond lengths and symmetrical stretching (breathing) frequencies of the reactants.[15] The equilibrium iron–oxygen distances for $Fe(H_2O)_6^{2+}$ and $Fe(H_2O)_6^{3+}$ determined crystallographically are 2.12 and 1.98 Å,[19] and the breathing frequencies of the complexes are 390 and 490 cm^{-1},[20,21] respectively. Since an exchange reaction is being considered, the two reactants and the two products have the same nuclear configurations (Fe–O distances) in the activated complex. The potential energy required to adjust the Fe–O distances in $Fe(H_2O)_6^{2+}$ and $Fe(H_2O)_6^{3+}$ to the activated complex value $d^* = (f_2 d_2^0 + f_3 d_3^0)/(f_2 + f_3)$[15] is given by

$$E^*_{in} = \frac{3 f_2 f_3 (d_2^0 - d_3^0)^2}{(f_2 + f_3)} \tag{10}$$

where d_2^0 and d_3^0 are the equilibrium metal–oxygen distances, and f_2 and f_3 are the breathing force constants of the two reactants ($f_i = 4\pi\bar{\nu}_i^2 c^2 \mu$ where $\bar{\nu}$ is the breathing frequency in cm^{-1} and μ, the reduced mass, is equal to the mass of a single water molecule). The free energy required to reorganize the inner-coordination shells is related to the potential energy for the reorganization by

$$\Delta G^*_{in} = E^*_{in} - RT \ln Q^*/\Pi_i Q_i \tag{11}$$

where the Q_i are vibrational partition functions. We see that $\Delta G^*_{in} \sim E^*_{in}$ provided that the vibration partition function ratio is close to unity.

The vertical energy E_{in} is the amount of energy required to change the Fe–O distances from their equilibrium values in $Fe(H_2O)_6^{2+}$ and $Fe(H_2O)_6^{3+}$ to the equilibrium values in $Fe(H_2O)_6^{3+}$ and $Fe(H_2O)_6^{2+}$, respectively. It is given by

$$E_{in} = 3(f_2 + f_3)(d_2^0 - d_3^0)^2 \tag{12a}$$

$$= E^*_{in}\left(4 + \frac{(f_3 - f_2)^2}{f_2 f_3}\right) \tag{12b}$$

It is apparent from eq 12b that the activation energy for inner-sphere reorganization is slightly less than one-quarter of the vertical distance between the potential-energy sufaces at the minimum in the reactants surface. For the $Fe(H_2O)_6^{2+}$–$Fe(H_2O)_6^{3+}$ exchange reaction $(E_{in} - 4E^*_{in})/4E^*_{in}$ amounts to 5.3% or ~0.5 kcal mol^{-1}.

The reason for the difference between E_{in} and $4E^*_{in}$ is that the potential-energy surface considered is not parabolic with respect to the reaction coordinate. Figure 2 shows contours of a number of different potential-energy surfaces, all corresponding to harmonic distortions of the reactants and products (the dashed line is the reaction coordinate in each case). Figure 2a shows the energy contours for an exchange reaction in which the two reactants have different breathing force constants. Figure 2b shows the contours when the two reactants have the same breathing force constants, and Figure 2c corresponds to the case where the two reactants do not change their force constants after electron transfer (this assumption is made in some of the quantum-mechanical treatments). In Figure 2b the reaction coordinate is a straight line, yielding the parabolic curves shown in Figure 1. In Figure 2a the point labeled e, which occurs at the midpoint of the line joining the two minima, satisfies the relationship $E_{in} = 4E_e$ and it is readily apparent that for this case $E^*_{in} < E_e$. Although the reaction coordinate in Figure 2c is not a straight line, the transition state and the equilibrium nuclear configurations of the reactants and products do lie on a straight line; thus $E_{in} = 4E^*_{in}$ also for the case depicted in Figure 2c. Since $E_{in} = 4E^*_{in}$ when the breathing force constants of the reactants are identical (Figure 2b) we define a reduced force constant f_{in} by

$$f_{in} = 2f_2 f_3/(f_2 + f_3) \tag{13a}$$

The value of the reduced force constant is, of course, independent

(17) Sutin, N. In "Bioinorganic Chemistry", Eichhorn, G. L., Ed.: American Elsevier: New York, 1973; Vol. 2, Chapter 19, p 611.

(18) Asterisks (*) rather than double daggers (‡) are used to distinguish the reorganization parameters defined here from the usual transition-state parameters, which are defined for a kT/h prefactor. Although E_{th} in eq 7a is also an asterisked quantity, for convenience the asterisk has been omitted. For a further discussion of the differences between asterisked and daggered quantites see, for example, Marcus, R. A.; Sutin, N. *Inorg. Chem.* **1975**, *14*, 213.

(19) Hair, N. J.; Beattie, J. K. *Inorg. Chem.* **1977**, *16*, 245. Bauer, W. H. *Acta Crystallogr.* **1964**, *17*, 1167. Montgomery, H.; Chastain, R. V.; Nalt, J. J.; Witowska, A. M.; Lingafelter, E. C. *Ibid.* **1967**, *22*, 775. Hamilton, W. C. *Ibid.* **1962**, *15*, 353.

(20) The metal–oxygen symmetrical stretching frequency of $Fe(H_2O)_6^{2+}$ is 390 cm^{-1}.[21] The stretching frequency of $Fe(H_2O)_6^{3+}$ has not been determined; however we have assumed that it is the same as the stretching frequency of $Cr(H_2O)_6^{3+}$ (490 cm^{-1}).[21] The assumption that the metal–oxygen stretching frequencies of first-row transition-metal ions are insensitive to the nature of the metal ion is supported by the data available for the 2+ ions: the stretching frequencies of $Ni(H_2O)_6^{2+}$, $Mn(H_2O)_6^{2+}$, and $Zn(H_2O)_6^{2+}$ lie between 360 and 405 cm^{-1}.

(21) Nakamoto, K. "Infrared and Raman Spectra of Inorganic and Coordination Compounds", 3rd ed.: Wiley-Interscience: New York, 1978.

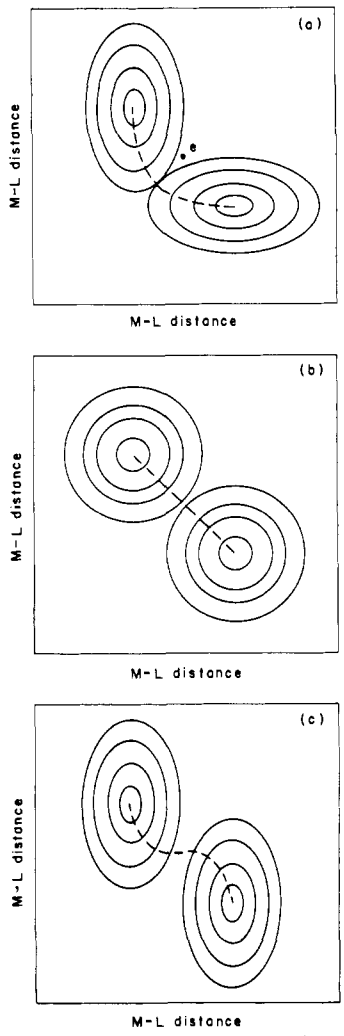

Figure 2. Energy contours of different potential-energy surfaces for electron-exchange reactions; the dashed line indicates the reaction coordinate. In (a) it is assumed that the two reactants have different symmetrical stretching frequencies and that these frequencies are interchanged upon electron transfer; in (b) it is assumed that the two reactants and the two products have the same symmetrical stretching frequency; in (c) it is assumed that the two reactants have different symmetrical stretching frequencies (as in case (a)), but that these frequencies do not change upon electron transfer. In each case the reaction coordinate is defined as the steepest descent path that connects the saddle point to the reactants' and products' potential-energy minima; this path is uniquely defined since the effective mass is the same for both coordinates.

of the oxidation state of the reactant, and replacing f_2 and f_3 in eq 10 by f_{in} does not change the value of E^*_{in}. In terms of f_{in}, E_{in} is given by

$$E_{in} = 4E^*_{in} = 6f_{in}(d_2^0 - d_3^0)^2 \qquad (13b)$$

We consider next the energy required to reorganize the solvent outside the inner coordination shells of the reactants. The expression for this reorganization energy, which has been derived by Marcus[3] and Hush[4] by using a continuum model for the solvent,[22-24] is

$$\Delta G^*_{out} = \frac{E_{out}}{4} = \frac{(\Delta q)^2}{4}\left(\frac{1}{2a_2} + \frac{1}{2a_3} - \frac{1}{r}\right)\left(\frac{1}{n^2} - \frac{1}{D_s}\right) \qquad (14)$$

where Δq is the charge transferred, a_2 and a_3 are the radii of the two reactants, r is the distance between the centers of the two reactants in the activated complex (generally taken equal to the close-contact distance $(a_2 + a_3)$ since this distance is assumed to correspond to the maximum rate), n is the refractive index, and D_s is the static dielectric constant of the medium. Since the continuum model does not allow for a change in the radii of the reactants, it is necessary to use an average reactant radius in eq 14.[25] For consistency, this radius is defined by $\bar{a} = 2a_2a_3/(a_2 + a_3)$, a definition which seems reasonable since it yields an $\bar{a}$ value which is very similar to the value obtained by using force-constant weighting.

To summarize, the electron transfer in the classical model is assumed to be adiabatic (that is, it is assumed that the reactants are converted into products with unit probability in the activated complex), and nuclear tunneling effects are neglected. The rate constant for electron transfer is given by

$$k_{el} = \nu_n e^{-(E_{out}+E_{in})/4RT} \qquad (15)$$

where E_{out} and E_{in} are temperature-independent reorganization energies and ν_n is an effective frequency for nuclear motion. In terms of the treatment of Dogonadze and co-workers,[10,24] this frequency is given by

$$\nu_n^2 = \frac{\nu_{out}^2 E_{out} + \nu_{in}^2 E_{in}}{E_{out} + E_{in}} \qquad (16)$$

Since metal–ligand stretching frequencies are typically 300–500 cm^{-1} while average solvent orientation frequencies are an order of magnitude lower,[22-24] $\nu_n/\nu_{in} \sim (E_{in}/(E_{out} + E_{in}))^{1/2}$ unless $E_{in} \ll E_{out}$.

We conclude this section by commenting on the difference between reorganization energies and reorganization free energies. In general, E is clearly defined as a temperature-independent energy difference on a potential-energy surface. The only ambiguity arises in the case of the continuous low-frequency solvent vibrations. In the process of making the connection between the ostensibly temperature-independent harmonic oscillator Hamiltonian and the dielectric continuum model for the solvent, Levich[6,26] ended up with a temperature-dependent solvent reorganization energy, which is, in fact, identical with the expression derived by Marcus (eq 14). The latter is clearly a free energy. However, since the actual temperature dependence of the reorganizational free energy of water is very small at room temperature this apparent inconsistency is of little consequence at room temperature. Thus, although the reorganization might have an entropy contribution so that, in general, $\Delta G^*_\lambda \neq E_{th}$, in the classical model this entropy contribution is assumed to be negligible. To the extent that this is true, ΔG^*_λ and E_{th} can be used interchangeably and eq 15 can be written as

$$k_{el} = \nu_n e^{-(\Delta G^*_{out}+\Delta G^*_{in})/RT} \qquad (17)$$

As will be seen, the use of the high-temperature model neglecting ΔS^*_λ turns out to be very useful in practice.

II. The Electronic Transmission Coefficient

In this section we introduce the electronic transmission coefficient. The use of this coefficient enables us to treat nonadiabatic reactions within the activated-complex framework, and provides a useful link between the classical and quantum-mechanical rate expressions.

The probability that the system will undergo a transition from one zero-order potential-energy surface to the other (in other

(22) The vibrational spectrum of water shows a number of bands.[23] The major band occurs at ~1 cm and satisfies the condition for a classical treatment of the solvent reorganization.[16] Note, however, that the spectrum of water also contains bands of higher frequency. More detailed treatments, which allow for the dispersion of solvent frequencies, have been presented;[6,10,16] for example, a correction factor of 0.87 to eq 14 is suggested in ref 10.

(23) Saxton, R. *Proc. R. Soc. London, Ser. A* **1952**, *213*, 473.

(24) Dogonadze, R. R. In "Reactions of Molecules at Electrodes", Hush, N. S., Ed.; Wiley-Interscience: New York, 1971; Chapter 3, p 135.

(25) The expression for E_{out} derived in ref 7 gives unrealistic values because the evaluation of the electric displacement vector for the reactants and products was based on different geometrics of the two ions in the reactant and product states. Although this, of course, corresponds to the actual situation, it is inconsistent with the electrostatic model used which is based upon charging arguments for cavities of fixed radii.

(26) As pointed out by Levich,[6] no quantity depending on macroscopic parameters such as temperature and solvent density can be contained in the quantum-mechanical Hamiltonian of the system.

words, that the reactants will be converted into products) on passing over the potential-energy barrier in Figure 1 is given by[16]

$$\kappa_{el} = 2P_{12}^0/(1 + P_{12}^0) \quad (18)$$

where P_{12}^0 is the probability of the reactants being converted into products per *single* passage through the intersection region. According to Landau[27] and Zener,[28] P_{12}^0 is given by

$$P_{12}^0 = 1 - e^{-4\pi^2 H_{AB}^2/h\upsilon|s_A - s_B|} \quad (19a)$$

where s_A and s_B are the slopes of the (zero-order) surfaces in the intersection region ($s_A = -s_B$ for an exchange reaction), and υ is the average velocity with which the system moves through the intersection region (υ is generally taken as the Boltzmann averaged velocity $(2RT/\pi\mu)^{1/2}$, where μ is the effective mass of the system). It is evident from eq 19a that $P_{12}^0 = 1$ when H_{AB} is large (strong coupling; the electron transfer is adiabatic), and that $P_{12}^0 \ll 1$ when H_{AB} is small (weak coupling; the electron transfer is nonadiabatic). Equation 19a is evaluated for a linear path tangent to the reaction coordinate at the crossing point (the general case is analogous to Figure 2c but with the two inner-sphere modes combined into a single mode and the remaining mode replaced by a solvent mode).[16] Substituting $\upsilon|s_A - s_B| = 4\nu_n(\pi RT(E_{out} + E_{in}))^{1/2}$ in eq 19a gives eq 19b. Expanding the exponential (nonadiabatic case) in eq 19b and substituting into eq 18 gives eq 20, which is the expression for κ_{el} for a nonadiabatic electron-exchange reaction. Finally, combining eq 5 (with $\Gamma_n = 1$) with eq 15, 18, and 20 gives eq 21.

$$P_{12}^0 = 1 - e^{-(H_{AB}^2/h\nu_n)(\pi^3/(E_{out}+E_{in})RT)^{1/2}} \quad (19b)$$

$$\kappa_{el} = \frac{2H_{AB}^2}{h\nu_n}\left(\frac{\pi^3}{(E_{out} + E_{in})RT}\right)^{1/2} \quad (20)$$

$$k_{el} = \frac{2H_{AB}^2}{h}\left(\frac{\pi^3}{(E_{out} + E_{in})RT}\right)^{1/2} e^{-(E_{out}+E_{in})/4RT} \quad (21)$$

If the classical rate constant expression eq 17 is used instead of eq 15, then the various substitutions give

$$k_{el} = \frac{2H_{AB}^2}{h}\left(\frac{\pi^3}{(E_{out} + E_{in})RT}\right)^{1/2} e^{-(\Delta G^*_{out}+\Delta G^*_{in})/RT} \quad (22)$$

Equations 21 and 22 are the expressions for the rate constant for a nonadiabatic electron-exchange reaction in the activated-complex framework. Note that these expressions no longer contain the nuclear vibration frequency; this frequency has been replaced by a prefactor that is essentially the frequency of electron transfer within the activated complex.[17]

III. Quantum-Mechanical Models

In the previous sections the electron transfer was described in terms of an activated-complex model. In this section we start from a quantum-mechanical treatment of nonadiabatic reactions. This treatment, which is based upon Fermi's golden rule, has been developed by Levich,[6] Dogonadze and co-workers,[10] Kestner, Logan, and Jortner,[7] Van Duyne and Fischer,[8] and Efrima and Bixon.[8]

According to Fermi's golden rule the probability per unit time that a system in an initial vibronic state Av will pass to a set of vibronic levels $\{Bw\}$ is given by[6,8]

$$W_{Av} = \frac{4\pi^2 H_{AB}^2}{h}\rho_w \quad (23)$$

$$\rho_w = \sum_w |\langle\chi_{Av}|\chi_{Bw}\rangle|^2\delta(\epsilon_{Av} - \epsilon_{Bw})$$

where H_{AB} is the electronic coupling matrix element introduced earlier, ρ_w is the weighted density of final states (i.e., the number of final states per unit energy interval weighted by the Franck–Condon factor $|\langle\chi_{Av}|\chi_{Bw}\rangle|^2$), ϵ_{Av} and ϵ_{Bw} are the unperturbed energies of the vibronic levels, and δ is the Dirac δ function that ensures energy conservation. It is assumed that only two electronic states, one for the reactants and one for the products, need to be considered. Assuming a Boltzmann distribution over the vibrational energy levels of the initial electronic state A, the thermally averaged probability per unit time of passing from a set of vibrational levels $\{Av\}$ of the initial electronic state to a set of vibrational levels $\{Bw\}$ of the final electronic state B is

$$W_A = \frac{1}{Q_A}\sum_v e^{-\epsilon_{Av}/RT} W_{Av} = \frac{4\pi^2 H_{AB}^2}{hQ_A}\sum_v\sum_w e^{-\epsilon_{Av}/RT}|\langle\chi_{Av}|\chi_{Bw}\rangle|^2\delta(\epsilon_{Av} - \epsilon_{Bw}) \quad (24)$$

where $Q_A = \sum_v e^{-\epsilon_{Av}/RT}$. Equation 24 is a general expression for the probability per unit time of a transition from an initial electronic state A to a final electronic state B. It is valid provided that the density of final states is large and the transition probability is small, that is, provided $W_A\tau \ll 1$, where τ is the duration of the perturbation causing the transition.[7]

Provided that the energy of the system can be expressed as a sum of contributions from the 2+ ion, the 3+ ion, and the solvent, the vibrational wave function can be expressed as a product of terms

$$\epsilon_{Av} = \epsilon^A_{2,k} + \epsilon^A_{3,l} + \epsilon^A_{s,m}$$

$$\epsilon_{Bw} = \epsilon^B_{2,p} + \epsilon^B_{3,q} + \epsilon^B_{s,r}$$

$$\chi_{Av} = \chi^A_{2,k}\chi^A_{3,l}\chi^A_{s,m}$$

$$\chi_{Bw} = \chi^B_{2,p}\chi^B_{3,q}\chi^B_{s,r}$$

where $(2,k)$, $(3,l)$, and (s,m) define the initial vibrational states of the 2+ ion, the 3+ ion, and the solvent, respectively (state A), and $(2,p)$, $(3,q)$ and (s,r) define their final vibrational states (state B). The rate constant for electron exchange is then

$$k_{el} = \frac{4\pi^2 H_{AB}^2}{Q_2Q_3Q_s} \times \sum_k\sum_l\sum_m\sum_p\sum_q\sum_r e^{-(\epsilon^A_{2,k}+\epsilon^A_{3,l}+\epsilon^A_{s,m})/RT}[S_{2,k;3,q}^2 S_{3,l;2,p}^2 S_{s,m;s,r}^2] \times \delta[(\epsilon^A_{2,k} + \epsilon^A_{3,l} + \epsilon^A_{s,m}) - (\epsilon^B_{2,p} + \epsilon^B_{3,q} + \epsilon^B_{s,r})] \quad (25)$$

where

$$Q_2 = \sum_k e^{-\epsilon_{2,k}/RT}$$

$$Q_3 = \sum_l e^{-\epsilon_{3,l}/RT}$$

$$Q_s = \sum_m e^{-\epsilon_{s,m}/RT}$$

$$S_{2,k;3,q}^2 = |\langle\chi_{2,k}|\chi_{3,q}\rangle|^2$$

$$S_{3,l;2,p}^2 = |\langle\chi_{3,l}|\chi_{2,p}\rangle|^2$$

$$S_{s,m;s,r}^2 = |\langle\chi_{s,m}|\chi_{s,r}\rangle|^2$$

Kestner, Logan, and Jortner[7] have shown that eq 25 reduces to eq 26 when the solvent modes are treated by a harmonic approximation in the high-temperature limit (i.e., classically; this assumption is justified since $h\nu_{out} < kT$ except at very low temperature[22]).

$$k_{el} = \frac{2H_{AB}^2}{hQ_2Q_3}\left(\frac{\pi^3}{E_{out}RT}\right)^{1/2}\sum_k\sum_l\sum_p\sum_q e^{-(\epsilon^A_{2,k}+\epsilon^A_{3,l})/RT}[S_{2,k;3,q}^2 S_{3,l;2,p}^2] \times e^{-(E_{out}+\Delta\epsilon)^2/4E_{out}RT} \quad (26)$$

where

$$\Delta\epsilon = (\epsilon^B_{2,p} + \epsilon^B_{3,q}) - (\epsilon^A_{2,k} + \epsilon^A_{3,l}) \quad (27a)$$

$$= (\epsilon^A_s - \epsilon^B_s) \quad (27b)$$

(27) Landau, L. *Phys. Z. Sowjetunion* **1932**, *2*, 46.
(28) Zener, C. *Proc. R. Soc. London, Ser. A* **1932**, *137*, 696; **1933**, *140*, 660.

Finally, it can be shown[7,29] that the high-temperature limit of eq 26 is eq 21, the semiclassical high-temperature limit for a nonadiabatic electron-exchange reaction. This is an important result, since, by use of the Landau–Zener equation, the quantum-mechanical approach (which is limited to the weak-coupling case) can be generalized to include any desired degree of electronic coupling.[6]

Although eq 26 has been derived assuming energy conservation in the electron-transfer step, it does not require that the inner-sphere and solvent modes conserve energy separately. Rather one mode can borrow energy from the other. This is allowed for by the last factor in the quadruple sum (the Gaussian term). Because of energy borrowing it is possible for the reactants' inner-sphere energy ($\epsilon^A_{2,k} + \epsilon^A_{3,l}$) to be considerably different from the products' inner-sphere energy ($\epsilon^B_{2,p} + \epsilon^B_{3,q}$) where $k \neq p$ and $l \neq q$. In fact, the Gaussian factor has its maximum value when $\Delta\epsilon = -E_{out}$, a condition that corresponds to a strongly exothermic inner-sphere change.

All of the terms in the sum of eq 26 have been evaluated for the $Fe(H_2O)_6^{2+}$–$Fe(H_2O)_6^{3+}$ exchange reaction by using either separate breathing frequencies of 390 and 490 cm^{-1} for $Fe(H_2O)_6^{2+}$ and $Fe(H_2O)_6^{3+}$, respectively, or the average frequency of 432 cm^{-1} defined by eq 13a.[30] The results of the two calculations do not differ significantly: the difference between the ΔG^*_λ (and ΔH^*_λ, see below) values calculated by the two methods is less than 0.02 kcal mol^{-1} over the temperature range 20–1500 K. The use of an average frequency instead of two separate frequencies means that the potential-energy contours are circular as in Figure 2b, rather than elliptical as in Figure 2a. As a consequence of the use of an average frequency the problem can be easily reformulated as a one-dimensional one since the reaction coordinate is now the straight line joining the two minima in the potential-energy surface (Figure 2b). Because a single frequency is being used, this line is a normal coordinate of the system, and the fluctuation leading to reaction is then a simple harmonic motion (the antisymmetric combination of breathing modes, with zero-point energy $h\nu_{in}/2$) along this coordinate. Under these conditions eq 26 can be reduced to a double sum:

$$k_{el} = \frac{2H_{AB}^2}{hQ_A}\left(\frac{\pi^3}{E_{out}RT}\right)^{1/2}\sum_m\sum_n e^{-\epsilon^A_m/RT}[S_{m,n}^2]e^{-(E_{out}+\Delta\epsilon)^2/4E_{out}RT} \quad (28)$$

where Q_A is a single-mode partition function, $\Delta\epsilon = (\epsilon^B_n - \epsilon^A_m)$, $\epsilon^A_m = m(h\nu_{in})$, and the $m(n)$ sum is over the reactant's (product's) quantum numbers associated with the normal coordinate defined above. The new Franck–Condon factor $S_{m,n}^2$ is defined in terms of the distance between the two minima in the potential-energy surface (Figure 2b), which is equal to $\sqrt{2}(d_2^0 - d_3^0)$.

The above formulation of the problem as a one-dimensional one using a single normal coordinate is, of course, identical with the two-dimensional problem based on the separate $Fe(H_2O)_6^{2+}$ and $Fe(H_2O)_6^{3+}$ breathing modes when both are assigned the same average frequency. The advantage of the single normal-mode formulation is that the calculations are simpler and closed-form expressions can be more readily derived. The calculations (using either eq 26 with the average frequency or eq 28) show that the root-mean-square value of $\Delta\epsilon$ at room temperature is 1.4×10^3 cm^{-1}. Since $\langle\Delta\epsilon\rangle_R$ is zero,[31] on the average the transition is to products that have either three quanta of vibrational energy more, or three quanta less, than the reactants. If the sum in eq 28 is restricted to terms for which $\Delta\epsilon = 0$, the calculated rate constant at 300 K is approximately 10% of the value obtained when all the terms are included.

The percentage of the total reaction at 300 K contributed by a pair of reactants with a particular inner-sphere energy ϵ^A_m in the reactive normal mode is shown in Figure 3. As expected, a

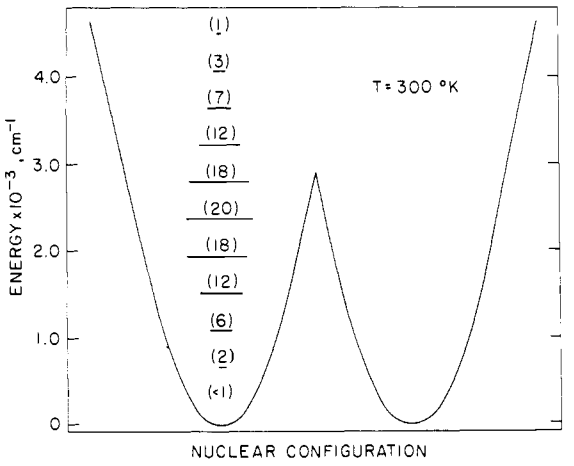

Figure 3. Percent contribution to the rate of the $Fe(H_2O)_2^{2+}$–$Fe(H_2O)_6^{3+}$ electron-exchange reaction at 300 K from reactants in a given vibrational level, calculated by using a one-dimensional model (eq 31b) with E_{out} = 25.6 kcal mol^{-1} (r = 6.9 Å), $(d_2^0 - d_3^0)$ = 0.14 Å, and $\bar{\nu}_{in}$ = 432 cm^{-1}.

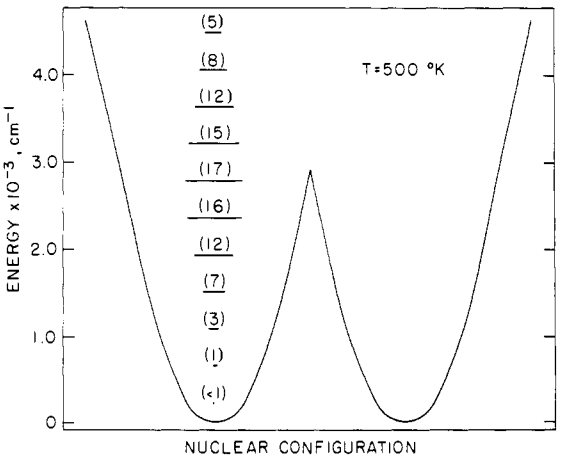

Figure 4. Percent contribution to the rate of the $Fe(H_2O)_6^{2+}$–$Fe(H_2O)_6^{3+}$ electron-exchange reaction at 500 K from reactants in a given vibrational level, calculated by using a one-dimensional model as for Figure 3.

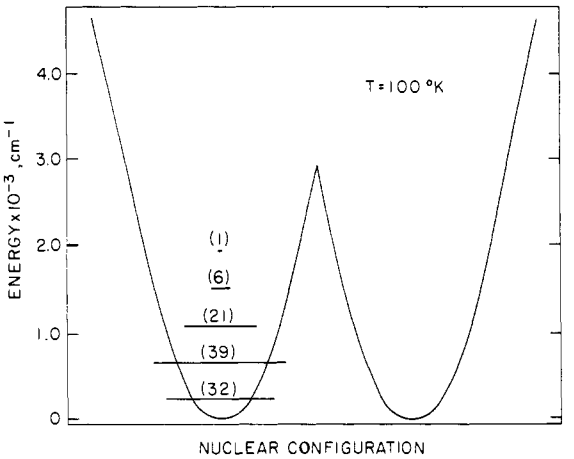

Figure 5. Percent contribution to the rate of the $Fe(H_2O)_6^{2+}$–$Fe(H_2O)_6^{3+}$ electron-exchange reaction at 100 K from reactants in a given vibrational level, calculated by using a one-dimensional model as for Figure 3.

(29) A single frequency for the breathing motions of the inner-coordination shells was used in deriving the high-temperature limit. The same high-temperature limit is obtained (numerically) for all of the cases depicted in Figure 2.

(30) The calculations were carried to high temperatures (1500 K) to show the convergence of the quantum-mechanical activation parameters to the classical values and are in no way intended to mimic the behavior of actual aqueous solutions. Accordingly, E_{out} was assumed to be temperature independent and the room-temperature values of D_s and n^2 were used. The Franck–Condon factors were calculated by using simple-harmonic-oscillator wave functions, with the metal–ligand stretching frequencies, the mass of the ligand, and the difference between the metal–ligand bond distances in the two oxidation states as parameters.

(31) See Appendix A.

Table I. Activation Parameters for the $Fe(H_2O)_6^{2+}$–$Fe(H_2O)_6^{3+}$ Electron Exchange Reaction Calculated by Using the Full Quantum Mechanical Model[a]

T, K	ΔG_λ^*, kcal mol^{-1}	ΔH_λ^*, kcal mol^{-1}	$-\Delta S_\lambda^*$, cal deg^{-1} mol^{-1}	ΔH_{in}^*, kcal mol^{-1}	ΔH_{out}^*, kcal mol^{-1}	$\langle \Delta E_{in}^a \rangle_R$, kcal mol^{-1}	$\langle \Delta E_{out}^a \rangle_R$, kcal mol^{-1}
20	7.46	6.40	52.92	0.01	6.39	0	6.38
40	8.52	6.41	52.59	0.03	6.38	0.01	6.36
60	9.54	6.57	49.57	0.20	6.37	0.17	6.34
80	10.48	7.02	43.19	0.65	6.37	0.61	6.33
100	11.26	7.71	35.53	1.34	6.37	1.29	6.33
150	12.61	9.64	19.80	3.27	6.38	3.19	6.31
200	13.36	11.14	11.09	4.77	6.38	4.65	6.29
250	13.79	12.14	6.58	5.76	6.38	5.62	6.28
300	14.05	12.81	4.15	6.42	6.39	6.25	6.26
350	14.22	13.25	2.76	6.87	6.39	6.67	6.24
400	14.33	13.57	1.91	7.18	6.39	6.95	6.22
450	14.42	13.79	1.38	7.40	6.39	7.15	6.20
500	14.48	13.96	1.03	7.57	6.39	7.29	6.18
550	14.52	14.09	0.79	7.70	6.39	7.39	6.16
600	14.56	14.19	0.61	7.80	6.39	7.46	6.13
650	14.58	14.27	0.49	7.87	6.39	7.51	6.11
700	14.60	14.33	0.39	7.94	6.39	7.54	6.09
750	14.62	14.38	0.32	7.99	6.39	7.56	6.07
1000	14.68	14.54	0.14	8.14	6.39	7.58	5.96
1500	14.72	14.65	0.04	8.26	6.40	7.41	5.75
2000	14.73	14.70	0.02	8.30	6.40	7.17	5.54
∞	14.77	14.77	0.0	8.37	6.40		

[a] Calculated from eq 28, using $(d_2^0 - d_3^0) = 0.14$ Å, $E_{out} = 25.6$ kcal mol^{-1} ($r = 6.9$ Å), and $\bar{\nu}_{in} = 432$ cm^{-1}.

significant portion of the reaction comes from reactants having insufficient inner-sphere energy to reach the classical transition state (2930 cm^{-1} or 8.4 kcal mol^{-1}). Figures 4 and 5 are similar to Figure 3 except that the temperatures are now 500 and 100 K, respectively. The rate changes by many orders of magnitude over this temperature range. At 500 K most of the reaction occurs from a vibrational level that is one quantum higher than the level contributing most of the reaction at 300 K. At 100 K most of the reaction occurs from the two lowest vibrational levels. Figures 3–5 thus provide a qualitative picture of the temperature dependence of the activation enthalpy and entropy expected for the quantum-mechanical model.

Activation Parameters. In order to obtain further information about the temperature dependence of the rate constants and for purposes of comparison with other models, thermodynamic activation parameters for the quantum-mechanical case can be defined as follows. The quantum-mechanical and semiclassical models converge at high temperatures (eq 26 and eq 21 and 22). This suggests an approach in which the semiclassical high-temperature expression is generalized by the introduction of a temperature-dependent inner-sphere reorganization energy:

$$k_{el} = \nu_n \kappa_{el} e^{-(\Delta G^*_{out} + \Delta G^*_{in}(T))/RT} \quad (29)$$

Remaining within the weak-coupling limit, κ_{el} in eq 29 can be replaced by the appropriate Landau–Zener expression to give

$$k_{el} = \frac{2H_{AB}^2}{h}\left(\frac{\pi^3}{(E_{out} + E_{in})RT}\right)^{1/2} e^{-(\Delta G^*_{out} + \Delta G^*_{in}(T))/RT} \quad (30)$$

Equation 30 is, of course, similar to eq 22 but it has been defined for all temperatures by using $\Delta G_{in}^*(T)$ in the exponent instead of ΔG_{in}^*. Comparison of eq 26 with eq 30 shows that $(\Delta G_{out}^* + \Delta G_{in}^*(T))$ is given by

$$e^{-(\Delta G^*_{out} + \Delta G^*_{in}(T))/RT} = \left(\frac{E_{out} + E_{in}}{E_{out}}\right)^{1/2} \frac{1}{Q_2 Q_3} \sum_k \sum_l \sum_p \sum_q e^{-(\epsilon^A_{2,k} + \epsilon^A_{3,l})/RT} [S_{2,k;3,q}^2 S_{3,l;2,p}^2] \times e^{-(E_{out} + \Delta\epsilon)^2/4E_{out}RT} \quad (31a)$$

The analogous equation for the one-mode case is

$$e^{-(\Delta G^*_{out} + \Delta G^*_{in}(T))/RT} = \left(\frac{E_{out} + E_{in}}{E_{out}}\right)^{1/2} \frac{1}{Q_A} \sum_m \sum_n e^{-\epsilon^A_m/RT} S_{m,n}^2 e^{-(E_{out} + \Delta\epsilon)^2/4E_{out}RT} \quad (31b)$$

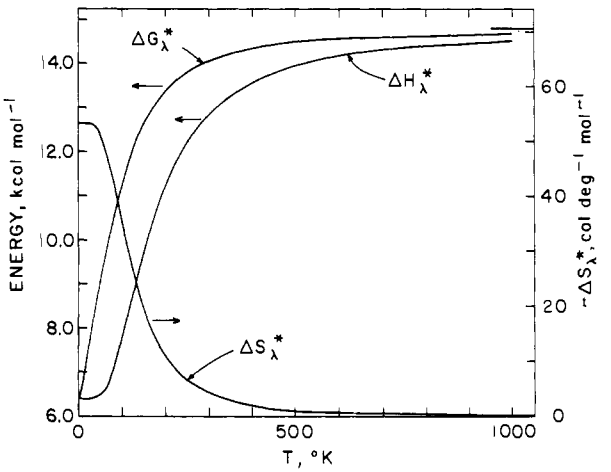

Figure 6. Plot of the activation parameters for the $Fe(H_2O)_6^{2+}$–$Fe(H_2O)_6^{3+}$ electron-exchange reaction vs. temperature calculated by using a one-dimensional model as for Figure 3. The horizontal line is the classical value of the activation energy and enthalpy.

The enthalpy and entropy contributions are readily obtained from the temperature dependence of $(\Delta G_{out}^* + \Delta G_{in}^*(T)) = \Delta G_\lambda^*$, using the Gibbs–Helmholtz equation.

The calculated values of ΔG_λ^*, ΔH_λ^*, and ΔS_λ^* for the $Fe(H_2O)_6^{2+}$–$Fe(H_2O)_6^{3+}$ exchange reaction are presented in Table I and plotted in Figure 6. As is required by the formalism, ΔH_λ^* and ΔG_λ^* approach their common classical value at high temperature. However, even at room temperature the difference between the quantum-mechanical and classical values is not large. Consistent with the information conveyed by Figure 3, a small amount of nuclear tunneling is reflected in the enthalpy, which is ~2 kcal mol^{-1} less than the classical value. The Franck–Condon factors also introduce a small negative entropy contribution at room temperature. The effects of the reductions in enthalpy and entropy of activation on the rate are in opposite directions and almost cancel. As a consequence the room-temperature rate is hardly affected by nuclear tunneling.

The calculated activation parameters for the $Fe(H_2O)_6^{2+}$–$Fe(H_2O)_6^{3+}$ exchange reaction are compared with the experimental values in Table II. There is fairly good agreement between the parameters calculated by using $(d_2^0 - d_3^0) = 0.14$ Å and the experimental values based upon the diffusional model for the

Table II. Comparison of Calculated and Experimental Activation Parameters for Electron Transfer within the $Fe(H_2O)_6^{2+}$|$Fe(H_2O)_6^{3+}$ Precursor Complex at 25 °C and Zero Ionic Strength

	$(d_2^0 - d_3^0)$, Å	ΔG_λ^*, kcal mol^{-1}	ΔH_λ^*, kcal mol^{-1}	ΔS_λ^*, cal deg^{-1} mol^{-1}
experimental[a,b] (diffusional)		14.9	13.5	−4.7
experimental[a,c] (collisional)		12.5	13.7	+4.1
classical[d]	0.14	14.8	14.8	0
classical[e]	0.11	11.6	11.6	0
quantum mechanical[f]	0.14	14.1	12.8	−4.2
quantum mechanical[g]	0.11	11.2	10.4	−2.5
semiclassical[h]	0.14	14.1	12.8	−4.2
semiclassical[i]	0.11	11.2	10.4	−2.5

[a] The experimental activation parameters have been extrapolated to zero ionic strength in the following manner. The measured rate constant of 4.2 M^{-1} s^{-1} at 25 °C and 0.55 M ionic strength (Silverman, J.; Dodson, R. W. *J. Phys. Chem.* 1952, *56*, 846) was corrected to zero ionic strength by using the extended Debye-Hückel equation with $d = 7$ Å and $c = -0.35$ M^{-1}. These parameters fit the iron(III)–vanadium(II) rate constants (Ekstrom, A.; McLaren, B. A.; Smythe, L. E. *Inorg. Chem.* 1976, *15*, 2853) at 0.1 and 1.0 M ionic strength. This procedure gives a rate constant of 0.14 M^{-1} s^{-1} corresponding to $\Delta G_0^{\ddagger} = 18.6$ kcal mol^{-1} for the $Fe(H_2O)_6^{2+}$–$Fe(H_2O)_6^{3+}$ reaction at 25 °C and zero ionic strength. The least-squares fit of all of the iron(III)–vanadium(II) kinetic data to the extended Debye-Hückel equation, using $1/\sigma^2$ weighting of the rate constants, gives $d = 13.5$ Å and $\Delta S_0^{\ddagger} = -22 \pm 3$ cal deg^{-1} mol^{-1}. Satisfactory fits could not be obtained with smaller d values since the calculated parameters were extremely sensitive to the weighting factors and d values used. Consistent behavior in the range 4–7 Å could, however, be obtained provided the fitting was restricted to the two lowest ionic strengths (0.1 and 1.0 M). This procedure gives $\Delta S_0^{\ddagger} \sim -30$ cal deg^{-1} mol^{-1}. For the present purposes we shall assume that $\Delta S_0^{\ddagger}$ for the $Fe(H_2O)_6^{2+}$–$Fe(H_2O)_6^{3+}$ exchange is equal to −22 cal deg^{-1} mol^{-1}, which is the $\Delta S_0^{\ddagger}$ value obtained from a linear extrapolation of the experimental $\Delta S^{\ddagger}$ values for the iron(III)–vanadium(II) reaction to zero ionic strength. Using the Gibbs-Helmholtz equation, $\Delta H_0^{\ddagger}$ for the exchange reaction at zero ionic strength is calculated to be 12.1 kcal mol^{-1}. [b] The experimental activation parameters for electron transfer within the precursor complex were extracted from the experimental data by using a diffusional model for the formation of the precursor complex (see ref 13, eq 20b and 21b). We call this the diffusional model, rather than the statistical model (as done, for example, in ref 11 and 13) because, as shown by Eigen (Eigen, M. *Z. Phys. Chem. (Frankfurt am Main)* 1954, *1*, 176), the equilibrium constant for the formation of the precursor complex can be expressed as the ratio of the forward and reverse diffusion rates, even though the diffusion coefficients do not appear in the final expression for the equilibrium constant. For this model, $k_{ex} = (4\pi Nr^3/3)(kT/h)\exp(-\Delta G_\lambda^*/RT)$ and $\Delta G_0^{\ddagger} = \Delta G_\lambda^* + \Delta G_0$, $\Delta H_0^{\ddagger} = \Delta H_\lambda^* + \Delta H_0$, and $\Delta S_0^{\ddagger} = \Delta S_\lambda^* + \Delta S_0$ where ΔG_0, ΔH_0, and ΔS_0 are 3.7 kcal mol^{-1}, −1.4 kcal mol^{-1}, and −17.3 cal deg^{-1} mol^{-1}. These values were calculated by using $D_s = 78.5$, $d \ln D_s/d \ln T = -1.37$, and $r = 6.9$ Å. [c] The experimental activation parameters were extracted as in footnote *b* except that a collisional model for the formation of the precursor complex was used (see ref 13, eq 20a and 21a). For this model, $k_{ex} = Z \times \exp(-\Delta G^*/RT)$ and $\Delta G_0 = 6.1$ kcal mol^{-1}, $\Delta H_0 = -1.6$ kcal mol^{-1}, and $\Delta S_0 = -26.1$ cal deg^{-1} mol^{-1}. These values were calculated by using $Z = 10^{11}$ M^{-1} s^{-1} and the other parameters in footnote *b*. [d] Calculated from eq 10 and 14, using $E_{out} = 25.6$ kcal mol^{-1} and $(d_2^0 - d_3^0) = 0.14$ Å. [e] Calculated from eq 10 and 14, using $E_{out} = 25.6$ kcal mol^{-1} and $(d_2^0 - d_3^0) = 0.11$ Å. [f] Calculated from eq 31, using $E_{out} = 25.6$ kcal mol^{-1} and $(d_2^0 - d_3^0) = 0.14$ Å. [g] Calculated from eq 31, using $E_{out} = 25.6$ kcal mol^{-1} and $(d_2^0 - d_3^0) = 0.11$ Å. [h] Calculated from eq 40 or 42, using $E_{out} = 25.6$ kcal mol^{-1} and $(d_2^0 - d_3^0) = 0.14$ Å. [i] Calculated from eq 40 or 42, using $E_{out} = 25.6$ kcal mol^{-1} and $(d_2^0 - d_3^0) = 0.11$ Å.

formation of the precursor complex.[11,13] To the extent that the diffusional model is correct, this agreement would seem to leave very little room for nonadiabaticity. However, recent EXAFS studies[32] indicate that the solution value of $(d_2^0 - d_3^0)$ is 0.11 Å,

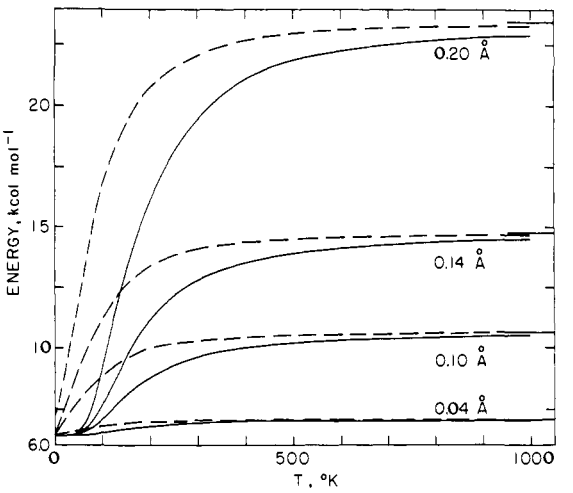

Figure 7. Plot of the activation parameters (dashed line, ΔG_λ^*; solid line, ΔH_λ^*) for electron-exchange reactions vs. temperature, calculated by using $E_{out} = 25.6$ kcal mol^{-1} ($r = 6.9$ Å), $\bar{\nu}_{in} = 432$ cm^{-1}, and $(d_2^0 - d_3^0) = 0.20$, 0.14, 0.10, and 0.04 Å, respectively. The horizontal lines are the classical values of the activation energy and enthalpy for the particular systems.

Table III. Percentage Reaction from the Lowest Vibrational Level as a Function of $(d_2^0 - d_3^0)$ and Temperature

	% reaction at $(d_2^0 - d_3^0)$			
T, K	0.04 Å	0.10 Å	0.14 Å	0.20 Å
40	99.9	99.5	99.1	98.1
100	91.6	57.6	32.6	8.6
300	53.1	5.2	0.2	0.0
500	35.8	3.2	0.1	0.0

[a] Calculated from eq 26, using $E_{out} = 25.6$ kcal mol^{-1} and $\bar{\nu}_{in} = 432$ cm^{-1}.

rather less than the value determined crystallographically (0.14 Å). If the EXAFS value is used, the agreement between the calculated parameters (assuming adiabaticity) and the experimental values based upon the diffusional model becomes poorer while the agreement with the values calculated with the collisional model improves. In view of the uncertainty in the values of $(d_2^0 - d_3^0)$ and of $\Delta S_0^{\ddagger}$ noted in footnote *a* of Table II, it is difficult to draw any firm conclusions about the importance of nonadiabaticity in the $Fe(H_2O)_6^{2+}$–$Fe(H_2O)_6^{3+}$ exchange reaction at this time. Calculations of H_{AB} that are currently in progress should help to resolve this situation.[33,34]

The effect of changing the inner-sphere barrier on the activation parameters is shown in Figure 7. The solvent barrier was kept constant ($E_{out} = 25.6$ kcal mol^{-1}, $r = 6.9$ Å) for all the calculations while the value of $(d_2^0 - d_3^0)$ was systematically varied. As expected, nuclear tunneling becomes more important as the difference between the metal–ligand bond distances increases. However the nuclear tunneling corrections to the room-temperature rates are again seen to be small, even for systems with large inner-sphere barriers.[35] Table III shows the percentage of the

(32) Sham, T. K.; Hastings, J. B.; Perlman, M. L. *J. Am. Chem. Soc.*, in press.

(33) Newton, M. D., work in progress, cited, in part, in ref 13. The results to date, based on direct iron–iron overlap, appear to give a reasonable account of the overall rate constant and suggest that there may well be an appreciable degree of nonadiabatic character.

(34) Newton, M. D. *Int. J. Quantum Chem., Symp.*, in press. Jafri, J. A.; Logan, J.; Newton, M. D. *Isr. J. Chem.*, in press (special issue on theory of molecular structure).

(35) Although the conclusion about the importance of nuclear tunneling at room temperature seems inconsistent with the calculations on the Co$(NH_3)_6^{2+}$–Co$(NH_3)_6^{3+}$ exchange reaction reported in ref 36, it should be noted that the authors of ref 36 compared the results of their quantum-mechanical calculation with the results of a classical calculation in which a different set of force constants had been used.

(36) Buhks, E.; Bixon, M.; Jortner, J.; Navon, G. *Inorg. Chem.* **1979**, *18*, 2014.

reaction that comes from the lowest vibrational level as a function of $(d_2^0 - d_3^0)$ and temperature. To put the values in perspective, one should note that $(d_2^0 - d_3^0)$ values for the $Co(NH_3)_6^{2+,3+}$, $Ru(H_2O)_6^{2+,3+}$, and $Ru(NH_3)_6^{2+,3+}$ exchange reactions are 0.18,[37] ~0.1,[38] and 0.04 Å,[37] respectively.

Further insight into the temperature dependence of the rate constants can be obtained by using the Tolman interpretation[39] of the activation energy. Provided that the rate constant is of the Arrhenius form (eq 32a with A temperature independent), the activation energy is given by eq 32b

$$k(T) = Ae^{-E_a/RT} \tag{32a}$$

$$E_a = \langle E \rangle_R - \langle E \rangle \tag{32b}$$

$\langle E \rangle_R$ is the average energy of all the reacting molecules,[40] and $\langle E \rangle$ is the average energy of all the molecules. The rate constants for the adiabatic reactions considered here are of this form (see, for example, the classical expression eq 6). On the other hand, as we have seen, the prefactor for nonadiabatic reactions is temperature dependent and the rate constant is of the form shown in eq 33. For nonadiabatic reactions the appropriate form of eq 32b is eq 34a

$$k(T) = BT^{-1/2}e^{-\Delta G^*_\lambda(T)/RT} \tag{33}$$

$$\Delta H^*_\lambda - RT/2 = \langle E^a_{in} \rangle_R + \langle E^a_{out} \rangle_R \tag{34a}$$

$$= (\langle E_{in} \rangle_R - \langle E_{in} \rangle) + (\langle E_{out} \rangle_R - \langle E_{out} \rangle) \tag{34b}$$

where $\langle E^a_{in} \rangle_R$ and $\langle E^a_{out} \rangle_R$ are the averaged inner- and outer-sphere reorganization energies, respectively. Differentiation of eq 31 shows that in the present case ΔH^*_λ is given by

$$\Delta H^*_\lambda = \langle E_{in} \rangle_R - \langle E_{in} \rangle + \frac{E_{out}}{4}\left\langle \left(1 + \frac{\Delta\epsilon}{E_{out}}\right)^2 \right\rangle_R \tag{35a}$$

where

$$\langle E_{in} \rangle = \frac{\sum_m \epsilon^A_m e^{-\epsilon^A_m/RT}}{\sum_m e^{-\epsilon^A_m/RT}}$$

and $\langle E_{in} \rangle_R$ is defined in footnote 40. Recalling that $\langle \Delta\epsilon \rangle_R = 0$, it follows from a comparison of eq 34a and eq 35a that the averaged outer-sphere reorganization energy is given by

$$\langle E^a_{out} \rangle_R = \frac{E_{out}}{4}\left(1 + \frac{\langle \Delta\epsilon^2 \rangle_R}{{E_{out}}^2}\right) - \frac{RT}{2} \tag{35b}$$

The calculated values of ΔH^*_λ, $\langle E^a_{out} \rangle_R$, and $\langle E^a_{in} \rangle_R$ are presented in Table I. As expected, ΔH^*_λ increases with increasing temperature, approaching the classical value of $(E_{in} + E_{out})/4$ at high temperature (compare eq 21 and 33). The small values of ΔH^*_λ at low temperatures reflect the contribution that nuclear tunneling makes to the rate. The values of $\langle E^a_{in} \rangle_R$ and $\langle E^a_{out} \rangle_R$, however do not equal the classical values at high temperature. This arises as follows. The high-temperature value of $\langle \Delta\epsilon^2 \rangle_R$ is given by eq 36a (Appendix B). Upon substituting this expression into eq 35b, the high-temperature value of the averaged outer-sphere reorganization energy is obtained (eq 36b). Combining this result with the high-temperature result $\Delta H^*_\lambda = (E_{in} + E_{out})/4$ gives eq 36c. The latter is the expression for the averaged inner-sphere reorganization energy in the high-temperature limit.

$$\langle \Delta\epsilon^2 \rangle_R = \frac{2RTE_{in}E_{out}}{E_{in} + E_{out}} \tag{36a}$$

$$\langle E^a_{out} \rangle_R = \frac{E_{out}}{4}\left(1 - \frac{2RT}{E_{in} + E_{out}}\right) \tag{36b}$$

$$\langle E^a_{in} \rangle_R = \frac{E_{in}}{4}\left(1 - \frac{2RT}{E_{in} + E_{out}}\right) \tag{36c}$$

It is evident from the above equations that the high-temperature values of $\langle E^a_{out} \rangle_R$ and $\langle E^a_{in} \rangle_R$ are less than the classical values $E_{out}/4$ and $E_{in}/4$, respectively, and that the difference increases with increasing temperature. This is a consequence of the fact that the former values were calculated from a nonadiabatic rate expression with a temperature-dependent prefactor, while the latter were calculated from an adiabatic rate expression with a temperature-independent prefactor. Note that $\langle E^a_{out} \rangle_R / \langle E^a_{in} \rangle_R = E_{out}/E_{in}$ in the high-temperature limit.

The above considerations suggest a procedure for partitioning ΔH^*_λ between ΔH^*_{in} and ΔH^*_{out} which is valid at all temperatures. Since $\Delta H^*_\lambda = (\Delta H^*_{in} + \Delta H^*_{out})$ it follows from eq 34a that

$$\Delta H^*_{in} + \Delta H^*_{out} = \langle E^a_{in} \rangle_R + \langle E^a_{out} \rangle_R + (RT/2) \tag{37a}$$

If it is now assumed that $RT/2$ can be partitioned between ΔH^*_{out} and ΔH^*_{in} by using $E_j/(E_{in} + E_{out})$ weighting, where j = out or in, respectively (as in eq 36b and 36c),[41] then ΔH^*_j and $\langle E^a_j \rangle_R$ are related by

$$\Delta H^*_{out} = \langle E^a_{out} \rangle_R + \frac{RT}{2}\left(\frac{E_{out}}{E_{in} + E_{out}}\right) \tag{37b}$$

$$\Delta H^*_{in} = \langle E^a_{in} \rangle_R + \frac{RT}{2}\left(\frac{E_{in}}{E_{in} + E_{out}}\right) \tag{37c}$$

Values of ΔH^*_{out} and ΔH^*_{in} calculated from eq 37 are included in Table I. The values of ΔH^*_{out} are seen to be essentially equal to $E_{out}/4$ throughout the entire temperature range. This is an important result since it shows that energy sharing between the inner-sphere and outer-sphere modes does not affect the solvent barrier defined in eq 37b.

IV. Nuclear Tunneling Factors

In this section we consider various procedures for correcting the classical rate expression for the effects of nuclear tunneling. As in the previous section, we consider that the nuclear tunneling corrections are only important for the inner-sphere modes and we define a nuclear tunneling factor (eq 38) as the ratio of the rate constant determined by the inner-sphere modes (including the effects of nuclear tunneling) to the high-temperature limit of this rate constant (i.e., its classical limit):

$$\Gamma_n = \frac{k_{in}(T)}{k_{in}(T=\infty)} = e^{-(4\Delta G^*_{in}(T) - E_{in})/4RT} \tag{38}$$

This procedure enables us to derive overall rate expressions that do not explicitly allow for energy sharing between the solvent and inner-shell modes. Its use is justified by the fact that, as noted above, the value of the solvent reorganization energy calculated with energy sharing does not differ significantly from the classical value of $E_{out}/4$ at any temperature (Table I). The average breathing frequency (defined by eq 13a) for the two oxidation states is again used since we have seen that no significant error is introduced by this procedure. This allows us to use the single normal-mode approach.

Following in the spirit of the quantum-mechanical treatment we use eq 23 to define the rate for a system to go from an initial state Av to a set of final states $\{Bw\}$ but we consider only the inner-sphere modes. We again Boltzmann average over a set of initial states $\{Av\}$ and assume that the energy can be written as a sum of terms for the two reactants. Proceeding as before and replacing the Dirac δ function by a Kronecker δ function divided

(37) Stynes, H. C.; Ibers, J. A. *Inorg. Chem.* **1971**, *10*, 2304.
(38) Estimated value. See: Böttcher, W.; Brown, G. M.; Sutin, N. *Inorg. Chem.* **1979**, *18*, 1447.
(39) Tolman, R. C. "Statistical Mechanics with Application to Physics and Chemistry"; Chemical Catalog Co.: New York, 1927; Chapter XXI.
(40) All average values denoted by a subscript R are defined by $\langle A \rangle_R = \sum_m \sum_n A k_{m,n} / \sum_m \sum_n k_{m,n}$ where $k_{m,n}$ is defined in Appendix A.
(41) This is equivalent to assuming that eq 36a is valid at all temperatures.

Table IV. Values of the Nuclear Tunneling Factor and Activation Parameters for the $Fe(H_2O)_6^{2+}$-$Fe(H_2O)_6^{3+}$ Electron Exchange Reaction Calculated by Using the Semiclassical Models

T, K	Γ_n[a]	ΔG^*_{in},[a] kcal mol^{-1}	ΔH^*_{in},[a] kcal mol^{-1}	$-\Delta S^*_{in}$,[a] cal deg^{-1} mol^{-1}	Γ_n[b]	ΔG^*_{in},[b] kcal mol^{-1}	ΔH^*_{in},[b] kcal mol^{-1}	$-\Delta S^*_{in}$,[b] cal deg^{-1} mol^{-1}
20	5.5×10^{79}	1.08	0.00	53.9	1.9×10^{80}	1.03	0.02	50.4
40	9.8×10^{33}	2.15	0.01	53.5	4.8×10^{34}	2.03	0.04	49.7
60	7.2×10^{18}	3.20	0.19	50.2	3.3×10^{19}	3.01	0.09	48.8
80	3.8×10^{11}	4.14	0.66	43.5	1.2×10^{12}	3.96	0.38	44.7
100	3.4×10^{7}	4.93	1.37	35.6	7.4×10^{7}	4.77	1.10	36.8
150	1.1×10^{3}	6.28	3.33	19.6	1.7×10^{3}	6.16	3.13	20.2
200	3.1×10^{1}	7.06	4.83	11.0	3.9×10^{1}	6.92	4.66	11.3
250	6.6	7.44	5.82	6.5	7.8	7.36	5.68	6.7
300	3.1	7.70	6.48	4.07	3.5	7.62	6.35	4.23
350	2.1	7.86	6.92	2.70	2.3	7.80	6.81	2.82
400	1.7	7.98	7.23	1.87	1.8	7.91	7.13	1.96
450	1.4	8.06	7.45	1.35	1.5	8.00	7.36	1.42
500	1.3	8.11	7.61	1.00	1.4	8.06	7.53	1.06
550	1.2	8.16	7.74	0.76	1.3	8.10	7.66	0.81
600	1.2	8.19	7.84	0.59	1.2	8.14	7.76	0.63
650	1.1	8.22	7.91	0.47	1.2	8.17	7.84	0.50
700	1.1	8.24	7.97	0.38	1.1	8.19	7.91	0.41
750	1.1	8.26	8.02	0.31	1.1	8.21	7.96	0.33
1000	1.0	8.31	8.18	0.13	1.1	8.27	8.12	0.15
1500	1.0	8.34	8.28	0.04	1.0	8.31	8.24	0.04
2000	1.0	8.36	8.32	0.02	1.0	8.32	8.28	0.02
2500	1.0	8.36	8.34	0.01	1.0	8.33	8.30	0.01
∞	1.0	8.37	8.37	0.0	1.0	8.37	8.37	0.0

[a] Calculated from eq 41 and 42, using $(d_2^0 - d_3^0) = 0.14$ Å and $\bar{\nu}_{in} = 432$ cm^{-1}. [b] Calculated from eq 40, using $(d_2^0 - d_3^0) = 0.14$ Å and $\bar{\nu}_{in} = 432$ cm^{-1}.

by $h\nu_{in}$, we obtain the following expression for the inner-sphere electron-transfer rate constant:

$$k_{in}(T) = \frac{4\pi^2 H_{AB}^2}{h^2 \nu_{in} Q_A} \sum_m e^{-\epsilon^A_m/RT} S_{m,m}^2 \qquad (39a)$$

Similar expressions have also been used by Jortner and Ulstrup[42] and by Laplante and Siebrand.[43] The high-temperature limit of eq 39a is eq 39b (compare eq 21 with $E_{out} = 0$) and the nuclear tunneling factor for this case is given by eq 39c.

$$k_{in}(T = \infty) = \frac{2H_{AB}^2}{h}\left(\frac{\pi^3}{E_{in}RT}\right)^{1/2} e^{-E_{in}/4RT} \qquad (39b)$$

$$\Gamma_n = \frac{(4\pi E_{in}RT)^{1/2}}{h\nu_{in}Q_A e^{-E_{in}/4RT}} \sum_m e^{-\epsilon^A_m/RT} S_{m,m}^2 \qquad (39c)$$

By analogy with the full quantum-mechanical case, the activation parameters are defined by

$$e^{-\Delta G^*_{in}(T)/RT} = \frac{(4\pi E_{in}RT)^{1/2}}{h\nu_{in}Q_A} \sum_m e^{-\epsilon^A_m/RT} S_{m,m}^2 \qquad (40)$$

with the activation enthalpy and entropy being obtained from the temperature dependence as before. Since the solvent is being treated classically, $\Delta G^*_{out} = \Delta H^*_{out} = E_{out}/4$, and $\Delta S^*_{out} = 0$. *This treatment yields activation parameters that are in excellent agreement with those obtained from the full quantum-mechanical treatment at all temperatures (20–1500 K; see Figure 8).* The calculated values of Γ_n are presented in Table IV.

Another approach is to use the closed-form expressions derived by Holstein.[5] Holstein starts with an expression that is the product of three factors: the rate of the system approaching the barrier, the tunneling probability, and a Landau–Zener-type factor. When this product is integrated over all positive velocities, Holstein obtains an expression which can be cast in the following form:[44]

$$k_{in}(T) = \frac{2H_{AB}^2}{h}\left(\frac{2\pi^3 \sinh\left(\frac{h\nu_{in}}{2kT}\right)}{E_{in}h\nu_{in}}\right)^{1/2} e^{-((E_{in}/h\nu_{in})\tanh(h\nu_{in}/4kT))} \qquad (41a)$$

The high-temperature limit of eq 41a is eq 39b, and the tunneling factor for this case is thus

$$\Gamma_n = \left(\frac{\sinh(h\nu_{in}/2kT)}{h\nu_{in}/2kT}\right)^{1/2} e^{-((E_{in}/h\nu_{in})\tanh(h\nu_{in}/4kT)-(h\nu_{in}/4kT))} \qquad (41b)$$

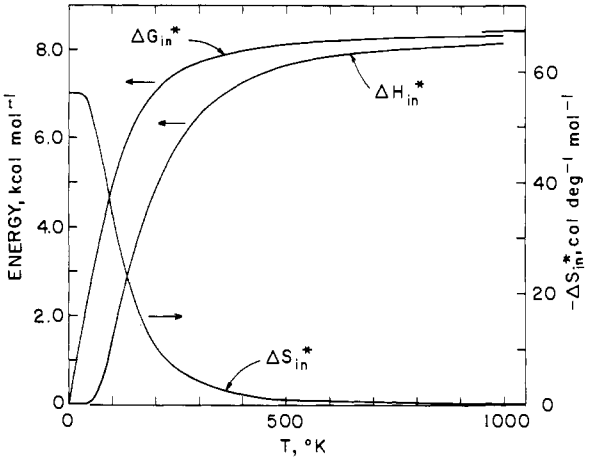

Figure 8. Plot of the inner-sphere activation parameters for the $Fe(H_2O)_6^{2+}$-$Fe(H_2O)_6^{3+}$ electron-exchange reaction vs. temperature calculated by using the semiclassical model with $(d_2^0 - d_3^0) = 0.14$ Å, $\bar{\nu}_{in} = 432$ cm^{-1}, and eq 40 or 42.

(42) Jortner, J.; Ulstrup, J. *Chem. Phys. Lett.* **1979**, *63*, 236.

(43) Laplante, J. P.; Siebrand, W. *Chem. Phys. Lett.* **1978**, *59*, 433. The high-temperature limit presented here (eq 39b) is different from the one given by Laplante and Siebrand (see their eq 10). The exponent in their expression is $(E_{in} - h\nu_{in})/4RT$; this exponent comes from an improper expansion of Z (defined in Appendixes B and C) as $(4a^2kT)\exp(-1/2kT)$ rather than as $4a^2kT$. Their prefactor is also incorrect by a factor of $\pi/2$.

(44) Equation 41a is valid over a larger temperature range than is the alternative semiclassical expression, eq II-26 of ref 7. This point has also been noted in ref 1 by Holstein in connection with the model proposed in ref 9.

Equation 41b can be derived from eq 39c by use of an asymptotic form of the modified Bessel function (see Appendix C).[45] Substitution of eq 41b into the semiclassical rate expression, eq 5, gives activation parameters that are in excellent agreement with those obtained by using the full quantum-mechanical expression at all but the lowest temperatures ($T < 80$ K). The main contribution to Γ_n comes from the exponential factor; in fact, *the agreement between the results obtained by using the full quantum-mechanical treatment and those given by eq 41b becomes excellent over the entire temperature range (Figure 7) when the prefactor in eq 41b is replaced by unity.* Using this modifed eq 41b, we can write relatively simple closed-form expressions for the inner-sphere activation parameters:

$$\Delta G^*_{in}(T) = E_{in}\left(\frac{kT}{h\nu_{in}}\right)\tanh\left(\frac{h\nu_{in}}{4kT}\right) \quad (42a)$$

$$\Delta H^*_{in}(T) = \frac{E_{in}}{4}\,\mathrm{sech}^2\left(\frac{h\nu_{in}}{4kT}\right) \quad (42b)$$

$$\Delta S^*_{in}(T) = \frac{E_{in}}{4T}\,\mathrm{sech}^2\left(\frac{h\nu_{in}}{4kT}\right)\left[1 - \left(\frac{2kT}{h\nu_{in}}\right)\sinh\left(\frac{h\nu_{in}}{2kT}\right)\right] \quad (42c)$$

Equation 42b is identical with the expression of Holstein[5] for the saddle-point energy, which is the energy at which the optimum compromise between activation and tunneling is achieved.

The above semiclassical expressions can be readily converted to the strong coupling limit (case (c) of the Introduction) by combining eq 42a with eq 29. Moreover, provided that $h\nu_{in} > 4kT$, eq 42 can be further simplified to give eq 43. The latter equation is a good approximation at temperatures below 150 K.[47]

$$\Delta G^*_{in}(T) = E_{in}\left(\frac{kT}{h\nu_{in}}\right) \quad (43a)$$

$$\Delta H^*_{in}(T) = \frac{E_{in}}{4}e^{-h\nu_{in}/2kT} \quad (43b)$$

$$\Delta S_{in}(T) = \frac{E_{in}}{4T}\left(e^{-h\nu_{in}/2kT} - \frac{4kT}{h\nu_{in}}\right) \quad (43c)$$

In summary, the modified Holstein equations can be used within the semiclassical framework to obtain closed-form expressions for the inner-sphere reorganization parameters. These expressions (together with $\Delta G^*_{out} = \Delta H^*_{out} = E_{out}/4$, and $\Delta S^*_{out} = 0$) give results that are essentially identical with those of the full quantum-mechanical treatment over the entire temperature range. This agreement justifies the use of the semiclassical approach developed here.

Conclusions

The semiclassical approach in which nonadiabaticity and nuclear tunneling factors are introduced as corrections to the classical expression gives results that are in excellent agreement with those yielded by the full quantum-mechanical treatment. This is an important conclusion since energy sharing between the inner-sphere and solvent modes is incorporated into the quantum-mechanical, but not into the semiclassical, model. As is apparent from the above, the energy-sharing terms give rise to the presence of (E_{in} + E_{out}) in the prefactor in the high-temperature form of the quantum-mechanical rate expression. In the separable semiclassical approach used here this prefactor is imposed at all temperatures through the Landau–Zener expression, with remarkable success.

The calculations show that nuclear tunneling effects are large at low temperature but that such effects are not important at room temperature unless the difference between the equilibrium configurations of the two oxidation states is extremely large. Over the entire temperature range the inner-sphere reorganization free energies and enthalpies are accurately given by the modified Holstein expressions (eq 42).

Appendix A

The value of $\langle\Delta\epsilon\rangle_R$ can be shown to be zero by the following argument. The average value of $\Delta\epsilon$ is defined by

$$\langle\Delta\epsilon\rangle_R = \frac{\sum_m\sum_n k_{m,n}\Delta\epsilon_{m,n}}{\sum_m\sum_n k_{m,n}} \quad (A1)$$

where

$$k_{m,n} = e^{-(\epsilon^A_m/RT)}[S_{m,n}{}^2]e^{-(\Delta\epsilon_{m,n}+E_{out})^2/4E_{out}RT} \quad (A2)$$

and the summation is from zero to infinity. If the last term in eq A2 is expanded and grouped with the first term, then

$$k_{m,n} = e^{-(\epsilon^A_m+\epsilon^B_n)/2RT}[S_{m,n}{}^2]e^{-((\Delta\epsilon_{m,n}{}^2/E_{out})+E_{out})/4RT} \quad (A3)$$

Consider the terms $k_{l,q}$ and $k_{q,l}$, where the reactants and products have interchanged their energy levels. Because of the assumption of the same force constants for all the reactants and products, $(\epsilon^A_l + \epsilon^B_q) = (\epsilon^A_q + \epsilon^B_l)$, $\Delta\epsilon_{l,q} = -\Delta\epsilon_{q,l}$, $(\Delta\epsilon_{l,q})^2 = (\Delta\epsilon_{q,l})^2$, and $S_{l,q}{}^2 = S_{q,l}{}^2$. This requires that $k_{l,q}$ be symmetric with respect to the interchange of l and q, i.e., $k_{l,q} = k_{q,l}$. Since $\Delta\epsilon_{l,q}$ is antisymmetric with respect to the interchange of l and q, the only terms that can make a net contribution to the numerator in eq A1 are the $l = q$ terms. But these terms are zero since $\Delta\epsilon_{l,l} = 0$. Therefore the numerator in eq A1 is zero, giving $\langle\Delta\epsilon\rangle_R = 0$.

Appendix B

Equation 36a can be derived as follows. Equation 26 can be converted to the equivalent expression[5,7]

$$k_{el} = A\sum_{m=-\infty}^{+\infty} e^{mh\nu_{in}/2kT}I_{|m|}(z)e^{-(E_{out}+mh\nu_{in})^2/4E_{out}RT} \quad (B1)$$

where the $I_{|m|}(z)$ are modified Bessel functions, $\Delta\epsilon = mh\nu_{in}$, $z = (E_{in}/h\nu_{in})\,\mathrm{csch}\,(h\nu_{in}/2kT)$, and

$$A = \frac{2H_{AB}{}^2}{h}\left(\frac{\pi^3}{E_{out}RT}\right)^{1/2}e^{-(z)\cosh(h\nu_{in}/2kT)}$$

Equation B1 can be rearranged to give

$$k_{el} = A'\sum_{-\infty}^{+\infty}k_m \quad (B2)$$

where

$$A' = Ae^{-E_{out}/4RT}$$

and

$$k_m = e^{-(mh\nu_{in})^2/4E_{out}RT}I_{|m|}(z)$$

Note that A and A' are not functions of m. From the definition of $\langle\Delta\epsilon^2\rangle_R$[40] it follows that

$$\langle\Delta\epsilon^2\rangle_R = \sum_m(mh\nu_{in})^2k_m/\sum_m k_m \quad (B3)$$

In the high-temperature limit, z and $I_{|m|}(z)$ can be replaced by

$$z = 2kTE_{in}/(h\nu_{in})^2$$

$$I_{|m|}(z) = \frac{1}{(2\pi z)^{1/2}}e^{(z-m^2/2z)}$$

and the sum can then be performed as an integral over m. This leads to the expression

$$\langle\Delta\epsilon^2\rangle_R = (h\nu_{in})^2\int \mathrm{d}m\; m^2e^{-\alpha m^2}/\int \mathrm{d}m\; e^{-\alpha m^2}$$

(45) If in eq 41b only the first two terms in the expansion of tanh ($h\nu_{in}/kT$) are retained, and the prefactor is replaced by unity, then the following expression presented previously by Nikitin[46] is obtained: $\Gamma_n = \exp[(E_{in}/h\nu_{in})(h\nu_{in}/4kT)^3/3]$.

(46) Nikitin, E. E. "Theory of Elementary Atomic and Molecular Processes in Gases"; Clarendon Press: Oxford, 1974; p 115. See also ref 13.

(47) At $T = 0$ K, $\Delta S_{in}{}^* = kE_{in}/h\nu_{in}$.

where

$$\alpha = (h\nu_{in})^2(E_{in} + E_{out})/4E_{in}E_{out}RT$$

Evaluation of this integral yields eq 36a.

Appendix C

The relationship between eq 39a and eq 41a can be shown as follows. Equation 39a can be rewritten as

$$k_{in} = \left(\frac{4\pi^2 H_{AB}^2}{h}\right)W \quad \text{(C1)}$$

where

$$W = \frac{1}{h\nu_{in}Q_A}\sum_{m=0}^{+\infty} e^{-mh\nu_{in}/kT}S_{m,m}^2 \quad \text{(C2)}$$

and

$$Q_A = \frac{1}{1 - e^{-h\nu_{in}/kT}}$$

The Franck–Condon factors can be expressed in terms of Laguerre polynomials[43,48]

$$S_{m,m}^2 = e^{-E_{in}/h\nu_{in}}\left(L_{m,m}\left(\frac{E_{in}}{h\nu_{in}}\right)\right)^2 \quad \text{(C3)}$$

Substitution in eq C2 gives

$$W = \frac{1 - e^{-h\nu_{in}/kT}}{h\nu_{in}}e^{-(E_{in}/h\nu_{in})}\sum_m (e^{-(h\nu_{in}/kT)})^m\left(L_{m,m}\left(\frac{E_{in}}{h\nu_{in}}\right)\right)^2 \quad \text{(C4)}$$

With the aid of the identity[49]

$$\sum_m y^m(L_{m,m}(x))^2 = \frac{1}{1-y}e^{-(2xy/(1-y))}I_0\left(\frac{2xy^{1/2}}{1-y}\right) \quad \text{(C5)}$$

where $I_0(2xy^{1/2}/(1-y))$ is a zero-order modified Bessel function, W can be rewritten as follows:

$$W = \frac{1}{h\nu_{in}}e^{-(E_{in}/h\nu_{in})(1+\exp(-h\nu_{in}/2kT)\operatorname{csch}(h\nu_{in}/2kT))}I_0(z)$$

where z has been defined in Appendix B. For large values of z (that is, at high temperatures)

$$I_0(z) = \frac{1}{(2\pi z)^{1/2}}e^z$$

and W becomes

$$W = \frac{1}{\left(2\pi E_{in}h\nu_{in}\operatorname{csch}\left(\frac{h\nu_{in}}{2kT}\right)\right)^{1/2}}e^{-E_{in}F/h\nu_{in}} \quad \text{(C6)}$$

where

$$F = 1 + e^{-h\nu_{in}/2kT}\operatorname{csch}\left(\frac{h\nu_{in}}{2kT}\right) - \operatorname{csch}\left(\frac{h\nu_{in}}{2kT}\right) \quad \text{(C7)}$$

Since

$$(\cosh(x) - 1)/\sinh(x) = \tanh(x/2)$$

the expression for F reduces to

$$F = \tanh\left(\frac{h\nu_{in}}{4kT}\right)$$

and therefore the expression for W is

$$W = \left(\frac{\sinh(h\nu_{in}/2kT)}{2\pi E_{in}h\nu_{in}}\right)^{1/2}e^{-(E_{in}/h\nu_{in})\tanh(h\nu_{in}/4kT)} \quad \text{(C8)}$$

Substitution of this expression into eq C1 gives eq 41a.

(48) Keil, T. H. *Phys. Rev. A* **1965**, *140*, 601.

(49) Copson, E. T. "Functions of a Complex Variable"; Oxford University Press: London, 1935; p 207.

Phosphole [2 + 2] and [4 + 2] Dimerizations around Metal Carbonyl Moieties. Structure and Chemistry of a New Type of Exo [4 + 2] Dimers

Catherine C. Santini,[1a] Jean Fischer,[1b] François Mathey,*[1a] and André Mitschler[1b]

Contribution from the Laboratoire CNRS-SNPE, B.P. No. 28, 94320 Thiais, France, and the Laboratoire de Cristallochimie, ERA 08, Institut Le Bel, Université Louis Pasteur, 67070 Strasbourg Cedex, France. *Received January 2, 1980*

Abstract: UV irradiation of mixtures of 3,4-dimethylphospholes (L) with $M(CO)_6$ (M=Cr, Mo, W) leads mainly to $(L\text{–}L)M(CO)_4$ complexes derived from Diels–Alder [4 + 2] phosphole dimers acting as chelating ligands. An X-ray structural study of one of these complexes shows that, contrary to normal endo phosphole dimers, these compounds have the exo configuration and that the phosphorus bridge is very strained: ∠CPC = 79.4°. With 1-phenylphosphole and $Mo(CO)_6$, the $(L\text{–}L)Mo(CO)_4$ complex has unexpectedly the structure of a [2 + 2] "head-to-head" dimer. At 50 °C the [4 + 2] dimeric complexes react with sulfur to yield the corresponding [4 + 2] exo dimeric phosphole sulfides, the spectral and chemical properties of which are compared with those of the corresponding endo dimeric sulfides. Contrary to the endo sulfides, the exo sulfides collapse at a relatively low temperature to yield a phosphinidene sulfide and a phosphindole derivative. Phenylphosphinidene sulfide thus prepared has been trapped by 2,3-dimethyl-1,3-butadiene to give a phospholene sulfide. Also based upon these observations, a two-step conversion of 1-phenylphosphole into 1-phenylphosphindole *P*-sulfide is described.

Weakly substituted λ^5 phospholes are known to dimerize instantly even at low temperature (eq 1). The structure of one such Diels–Alder dimer has been studied by X-ray.[2] The most interesting features are (1) the endo configuration at the junction

0002-7863/80/1502-5809$01.00/0